

4-2010

Ultrafast Carrier Dynamics In Type II ZNSE/CDS/ZNSE Nanobarbells

Nishshanka N. Hewa-Kasakarage

Patrick Z. El-Khoury

Alexander N. Tarnovsky


Bowling Green State University, atarnov@bgsu.edu

Maria Kirsanova

Ian Nemitz

See next page for additional authors

Follow this and additional works at: https://scholarworks.bgsu.edu/chem_pub

 Part of the [Chemistry Commons](#)

Repository Citation

Hewa-Kasakarage, Nishshanka N.; El-Khoury, Patrick Z.; Tarnovsky, Alexander N.; Kirsanova, Maria; Nemitz, Ian; Nemchinov, Alexander; and Zamkov, Mikhail, "Ultrafast Carrier Dynamics In Type II ZNSE/CDS/ZNSE Nanobarbells" (2010). *Chemistry Faculty Publications*. 52.
https://scholarworks.bgsu.edu/chem_pub/52

This Article is brought to you for free and open access by the Chemistry at ScholarWorks@BGSU. It has been accepted for inclusion in Chemistry Faculty Publications by an authorized administrator of ScholarWorks@BGSU.

Author(s)

Nishshanka N. Hewa-Kasakarage, Patrick Z. El-Khoury, Alexander N. Tarnovsky, Maria Kirsanova, Ian Nemitz, Alexander Nemchinov, and Mikhail Zamkov

Ultrafast Carrier Dynamics in Type II ZnSe/CdS/ZnSe Nanobarbells

Nishshanka N. Hewa-Kasakarage,^{S,⊥} Patrick Z. El-Khoury,^{†,*,⊥} Alexander N. Tarnovsky,^{†,*,*} Maria Kirsanova,^{†,S} Ian Nemitz,^S Alexander Nemchinov,^S and Mikhail Zamkov^{†,S,*}

[†]The Center for Photochemical Sciences, [‡]Department of Chemistry, and ^SDepartment of Physics, Bowling Green State University, Bowling Green, Ohio 43403. [⊥]These authors contributed equally to this work.

Colloidal synthesis of heterostructured semiconductor nanocrystals (NCs) offers a facile route for integrating multiple materials with different properties into a single nanoscale object, where the spatial localization of carriers can be precisely controlled by manipulating shapes and sizes of individual components.^{1,2} Recently, a great deal of work on the synthesis of composite semiconductor NCs has been focused on type II heterostructures, constructed from the two materials for which both the valence and conduction bands of one component lie lower in energy than the corresponding bands of the other component. The resulting staggered alignment of band edges at the heterostructured interface leads to an efficient spatial separation of electrons and holes, which presents attractive opportunities for utilization of these materials as charge-separating units in photovoltaic and photocatalytic applications.³

To date, compelling evidence of photoinduced charge separation in semiconductor nanocomposites has been provided for a large number of heterostructures including symmetric core/shell^{4–14} as well as more complex dot-in-a-rod,^{15–17} barbells,^{18–20} heterodimers,^{21,22} tetrapods,²³ and multi-branched structures.²⁴ While, the core/shell geometry is not fully optimized for photovoltaic applications because one of the carriers is always confined to the core of the nanoparticle, asymmetric heterostructures are highly suitable for photochemical conversion of light, as both nanocrystalline domains are exposed to the external environment allowing photogenerated carriers to undergo a charge transfer reaction with an electrolyte or a substrate. Within this group of materials, the carrier separation efficiency is primarily determined by the rate of photoinduced

ABSTRACT We employ femtosecond transient absorption spectroscopy to get an insight into ultrafast processes occurring at the interface of type II ZnSe/CdS heterostructured nanocrystals fabricated *via* colloidal routes and comprising a barbell-like arrangement of ZnSe tips and CdS nanorods. Our study shows that resonant excitation of ZnSe tips results in an unprecedentedly fast transfer of excited electrons into CdS domains of nanobarbells (<0.35 ps), whereas selective pumping of CdS components leads to a relatively slow injection of photoinduced holes into ZnSe tips ($\tau_h = 95$ ps). A qualitative thermodynamic description of observed electron processes within the classical limit of Marcus theory was used to identify a specific charge transfer regime associated with the ultrafast electron injection into CdS. Potential photocatalytic applications of the observed fast separation of carriers along the main axis of ZnSe/CdS barbells are discussed.

KEYWORDS: solar cells · nanocrystals · photovoltaics · type II · nanorods

charge transfer across the heterostructured interface, which depends on a number of system-specific parameters, such as quality of the epitaxial interface, carrier momentum in each nanocrystalline domain, the degree of band bending, and carrier trapping at the interface. Since most of these variables are *a priori* unknown, real time spectroscopic investigations of carrier dynamics in heterostructured nanocrystals are exceedingly important for understanding the ensuing charge transfer properties and ultimately the material's potential for light harvesting applications.

The dynamics of charge carriers in type II heterostructured NCs utilizing asymmetric arrangement of the two domains has been extensively investigated in recent years by means of ultrafast pump–probe spectroscopies.^{17,25–28} For instance, Peng *et al.*²⁵ have used femtosecond transient absorption (TA) spectroscopy to study electron processes in CdSe/CdTe nanotetrapods and have identified carrier cooling dynamics for interband, band-edge, and intraband transitions. CdSe/CdTe heterostructures in a barbell-like arrangement were subsequently studied in the group of Fiebig,²⁶

*Address correspondence to zamkovm@bgsu.edu.

Received for review September 21, 2009 and accepted March 17, 2010.

Published online March 25, 2010. 10.1021/nn100229x

© 2010 American Chemical Society

where evidence of fast, subpicosecond carrier transfer between CdSe and CdTe domains was presented. Finally, a recent report by Lupo *et al.*²⁷ has identified an ultrafast (650 fs) localization of holes in quasi-type II CdSe/CdS heterostructures, which was attributed to a reduced electron–hole Coulomb interaction associated with spatially separated excitons.

Here we investigate the ultrafast dynamics of charge carriers in type II ZnSe/CdS heterostructures comprising a barbell-like arrangement of ZnSe spheres and CdS nanorods,²⁰ fabricated *via* colloidal routes. Excited state population ratios for both materials were obtained from femtosecond transient absorption measurements through careful evaluation of the Stark effect and state-filling contributions into observed bleach recovery traces. We found that resonant excitation of ZnSe tips results in an ultrafast transfer (<0.35 ps) of excited carriers into CdS domains, whereas resonant pumping of CdS portions of barbells leads to a relatively slow injection of photoinduced holes into ZnSe domains ($\tau_{\text{h}} = 95$ ps). The observed interfacial electron transfer occurring under resonant pumping conditions is faster than previously reported for CdSe/CdTe²⁶ and CdSe/CdS²⁷ heterostructures, despite the large spatial delocalization of corresponding wave functions across the ZnSe/CdS heterojunction. This phenomenon is attributed to the near-epitaxial relationship between ZnSe and CdS crystalline domains, which is expected due to a relatively small (2.7%) lattice mismatch between merging lattices that helps relieve the interfacial strain, and consequently reduces the amount of interfacial defects.

Fast spatial separation of photoinduced charges along the main axis of ZnSe/CdS barbells, as well as the availability of both carriers for a chemical reaction with external media can be utilized by a number of optoelectronic applications. For instance, the ZnSe/CdS combination of materials is particularly well suited for photocatalytic water splitting since the electrochemical potentials of electrons and holes in ZnSe/CdS barbells straddle the $\text{H}_2/\text{H}_2\text{O}$ and $\text{O}_2/\text{H}_2\text{O}$ redox potentials.²⁹ In addition, fast charge transfer between ZnSe and CdS domains can be harnessed in applications that rely on a photoinduced electric dipole to modulate the spectral response of the material (e.g., electroabsorption switching and modulation³⁰), as was previously demon-

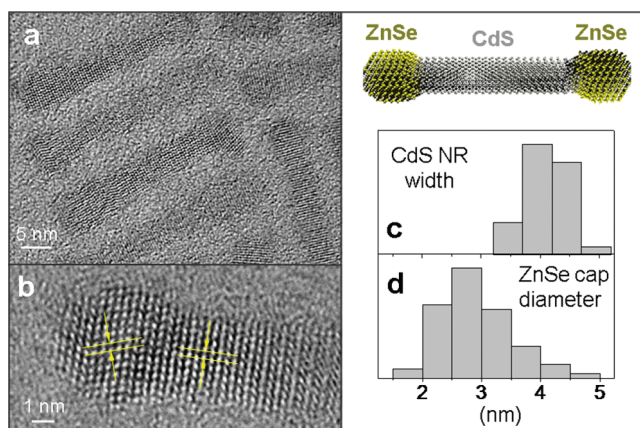


Figure 1. Structural analysis of ZnSe/CdS barbells: (a) high resolution transmission electron microscope (TEM) images of ZnSe/CdS heterostructures; (b) typical ZnSe/CdS barbell showing unique directions of lattice planes for each of the material domains; (c) statistical distributions of barbell widths; and (d) diameters of ZnSe tips.

strated for ZnSe/CdS nanorods exhibiting a photoinduced shift of the emission wavelength due to the quantum confined Stark effect.¹⁷ In the case of ZnSe/CdS barbells, the observed subpicosecond electron transfer can enable switching rates of up to 1–2 terahertz, which exceed the present day characteristics of Ge-based electroabsorption modulators by an order of a magnitude.³¹

RESULTS AND DISCUSSION

Motion of excitons in the ZnSe and CdS domains of a barbell structure is confined in the three and two dimensions, respectively, with a corresponding degree of confinement being determined by the size of ZnSe tips and widths of CdS NRs. Accurate determination of these parameters prior to spectroscopic characterization of the system is thus critical for establishing expected carrier energies in both materials. Average sizes of ZnSe and CdS domains are first estimated from high-resolution (HR) transmission electron microscopy (TEM) measurements. Figure 1a,b shows typical HR-TEM images of several ZnSe/CdS heterostructures, where the

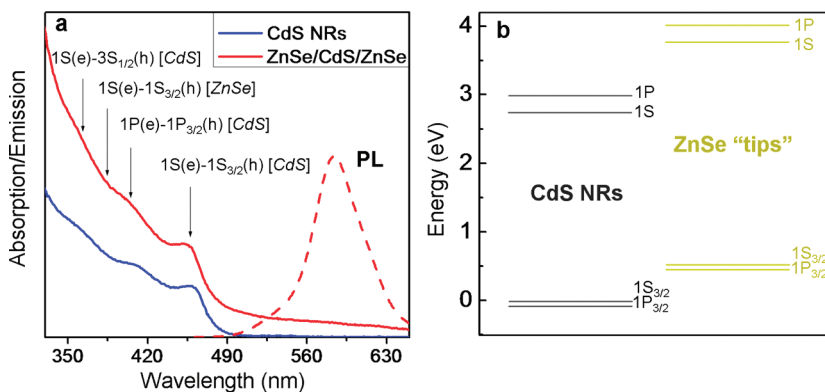


Figure 2. Determination of excited state energies in ZnSe/CdS heterostructures. (a) Steady-state absorption and emission ($\lambda_{\text{excitation}} = 420$ nm) spectra of ZnSe/CdS barbells (red) and CdS NRs (blue). Four lowest-energy excited state transitions are identified in the absorption spectra. (b) Calculated excited state energies for ZnSe/CdS heterostructures comprising 4.1-nm-wide CdS NRs and 2.85-nm ZnSe tips.

barbell-like arrangement of materials can be distinguished by the unique direction of lattice planes in ZnSe tips relative to those in the CdS NRs. Statistical analysis of approximately one hundred of such barbells shows a 5.7-nm elongation of these structures along the 001 axis in comparison with CdS NRs used for seeding the growth of ZnSe tips. Subtracting the mean length of CdS NRs from that of ZnSe/CdS barbells yields the average ZnSe diameter of 2.85 nm, which is consistent with the 2.89-nm average tip size determined from the measurements of individual heterostructures. The average width of barbells was found to be 4.1 nm, with the standard deviation of 0.34 nm (8%).

Steady-state absorption measurements confirm the narrow distribution of barbell widths, as evident from well-pronounced excitonic features corresponding to $1S(e) - 1S_{3/2}(h)$ and $1P(e) - 1P_{3/2}(h)$ transitions in CdS (Figure 2a). The band edge absorption in the ZnSe portion of barbells, which spectral position is expected³² to peak at 384 nm, is not resolved, possibly due to a relatively small volume fraction of the ZnSe phase in a barbell structure. Nevertheless, evidence of carrier absorption across the band gap of ZnSe is provided by the noticeable change in the slope of the absorption curve below 380 nm and the apparent bleaching of the band edge transition in time-resolved TA measurements (Figure 3c).

The relative alignment of $n = 1$ excited state energies in each component of the ZnSe/CdS heterostructure was calculated using known effective carrier masses^{33,34} (see the Supporting Information), optical absorption measurements, and TEM analysis of average domain sizes, as illustrated in Figure 2b. Further splitting of excitonic levels due to exchange interaction was not considered in this work since the overlap of electron and hole wave functions, which is proportional to the exchange term, is small in type II systems. According to Figure 2b, excited electrons find the minimum of the conduction band in the $1S(e)$ state of CdS NRs, which is positioned 0.80 eV lower than the $1S(e)$ energy of ZnSe tips, meanwhile photoinduced holes are expected to localize in the $1S_{3/2}(h)$ level of the ZnSe domain, which lies 0.53 eV above the valence band edge of CdS NRs. The energy of the spatially indirect transition associated with the recombination of carriers across the ZnSe/CdS interface is thus lower than the band gap of either ZnSe or CdS materials, which is consistent with the red-shifted emission of ZnSe/CdS heterostructures ($\hbar\omega = 2.1$ eV), shown in Figure 2a.

The photoinduced filling of excited states in NCs leads to bleaching of interband optical transitions, such that absorption changes are proportional to the number of excited carriers:

$$\Delta A(\hbar\omega) = - \sum_i A_{0,i}(\hbar\omega - \hbar\omega_i)(n_i^e + n_i^h) \quad (1)$$

where $A_{0,i}$ is an absorption profile of the i th transition, and n_i^e and n_i^h are occupation numbers of electron and hole states involved in the transition. Since the effective masses of holes in CdS and ZnSe materials are approximately 4–5 times greater than those of electrons, their room-temperature occupation probabilities are small. As a result, the state-filling-induced absorption changes are dominated by electrons.³⁵ The contribution of holes into bleaching is further reduced due to exchange interaction that splits the $1S$ exciton into two different hole states,^{36,37} such that the higher energy absorbing transition stays unoccupied until the lower energy hole state is completely filled, which occurs only when $\langle N \rangle \gg 1$.

Another possible contribution into bleaching of NC optical transitions is due to local fields that modify transient spectra *via* Stark effect.³⁸ This leads to a spectral shift of absorbing transitions as well as changes in the corresponding oscillator strengths resulting from modifications in selection rules. For systems exhibiting spatial separation of charges, such as barbell nanostructures investigated here, the contribution of the Stark effect can be particularly significant, and its evaluation is important in retrieving the state filling dynamics. As a semiempirical approach to predicting the spec-

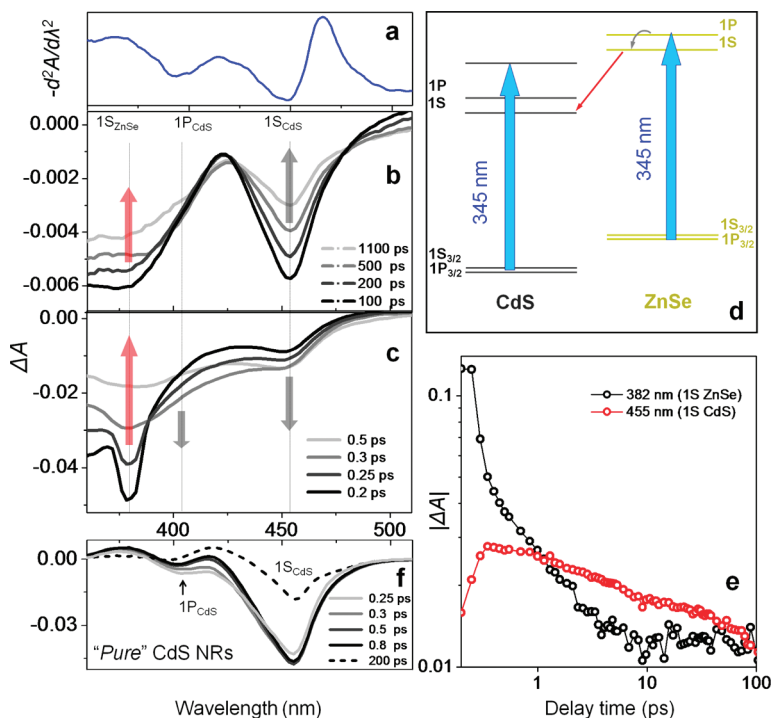


Figure 3. TA measurements of ZnSe/CdS barbells resulting from resonant excitation of ZnSe domains ($\lambda_{\text{pump}} = 345$ nm): (a) second derivative of the absorption profile; (b and c) TA spectra, $\Delta A = A(\text{pump} + \text{probe}) - A(\text{probe})$, corresponding to long (b) and short (c) delay times; (d) energy diagram of electronic states showing the maximum energy of pump photons (blue arrows) under resonant excitation of ZnSe domains; (e) temporal dynamics of the TA bleach recovery measured for band-edge excitons in CdS (red) and ZnSe (black) materials; (f) TA spectra of pure CdS NRs ($\lambda_{\text{pump}} = 345$ nm).

tral changes in the TA measurements of ZnSe/CdS barbells resulting from the Stark effect, we rely on the previously reported formalism^{39,40} that correlates the effect of carrier-induced local fields in semiconductor NCs with a repulsion between close-spaced transitions, such that the Stark effect contribution into ΔA is approximately equal to the second derivative of the absorption profile.

The transient absorption spectroscopy of hexane-suspended ZnSe/CdS barbells was performed using two excitation regimes that correspond to the resonant pumping of the $n = 1$ transitions in CdS and ZnSe domains of the structure. TA spectra resulting from the quasi-resonant excitation of ZnSe tips are analyzed in Figure 3. The wavelength of the pump beam, in this case, was set to 345 nm, which allows accessing the two low energy transitions in the ZnSe domain: $1S(e) - 1S_{3/2}(h)$ and $1P(e) - 1P_{3/2}(h)$, denoted as $1S_{ZnSe}$ and $1P_{ZnSe}$, respectively, as well as three lowest transitions in CdS NRs: $1S(e) - 1S_{3/2}(h)$, $1P(e) - 1P_{3/2}(h)$, and $1S(e) - 3S_{1/2}(h)$, as shown in the energy diagram (Figure 3d). Bleaching of band edge transitions in both materials was observed within 200 fs after excitation (Figure 3c) with spectral positions of bleach signals near the predicted energies of $1S_{ZnSe}$ and $1S_{CdS}$ excitons (Figure 2).

The contribution of the Stark effect into observed TA bleach signals is estimated by comparing the second derivative of the absorption spectra (Figure 3a) with the early time transient spectra (Figure 3c), revealing, at first glance, a similarity in corresponding slopes both in the case of CdS (450–465 nm) and ZnSe (385–405 nm) transitions. However, if the early time bleach has a significant contribution from the local fields, then the two maxima of d^2A/dt^2 would coincide with the photoinduced absorption ($\Delta A > 0$) in the TA spectra, which is not observed here, (ΔA remains negative throughout the entire spectral window of the probe beam). Furthermore, the initial modification of transition energies associated with the Stark effect typically recovers within a few picoseconds, causing a noticeable shift of the bleach minima, yet, in present measurements, spectral positions of $1S_{CdS}$ (450–465 nm) and $1S_{ZnSe}$ (370–395 nm) transitions are nearly constant within the entire nanosecond delay range (Figure 3b). In view of these observations, we conclude that the Stark effect on TA spectra is negligible, and the observed TA bleach is attributed primarily to state filling in ZnSe and CdS domains.

The subpicosecond bleach recovery resulting from the 345-nm excitation (Figure 3c) shows an interesting trend. In contrast to a rapid decay of carrier population occupying the lowest-energy $1S$ excitons of ZnSe, the bleach signal of the band edge transition in CdS is increasing during the 0.2–0.5 ps time window, as indicated by a gray arrow in Figure 3c. The observed rise in the populations of $1S_{CdS}$ excitons can be partly attributed to the relaxations of “hot” electrons from higher-

lying states, such as $1P_{CdS}$, since the energy of pump photons, in principle, is sufficient to induce absorption in any transition with energy below that of $1S(e) - 3S_{1/2}(h)$. TA absorption measurements performed on “pure” CdS nanorods (Figure 3f) confirm that the rise in the population of $1S_{CdS}$ excitons is correlated with the recovery of $1P_{CdS}$ bleach. The magnitude of the $1S_{CdS}$ rise for pure CdS NRs, however, is smaller than that for ZnSe/CdS barbells, which indicates that the $1S(e)$ level of ZnSe/CdS barbells receives carriers from transitions other than $1P_{CdS}$. The only electronic state that has the sufficient electron population at $\Delta t > 200$ fs and is energetically allowed to feed the $1S(e)$ level of CdS, is the conduction band edge of the ZnSe domain (see Figure 3d). Indeed, under resonant pumping conditions, valence electrons are being channeled into the $1S(e)$ state of ZnSe, which causes immediate bleaching of the $1S_{ZnSe}$ transition. These carriers can then undergo relaxation into the lower-lying $1S(e)$ and possibly $1P(e)$ states of CdS, leading to a rapid recovery of the $1S_{ZnSe}$ bleach (since the remaining holes in ZnSe do not contribute significantly into ΔA), and the simultaneous rise in $1S_{CdS}$ bleach signal. Such ultrafast electron transfer is consistent with significant driving force at the interface of ZnSe and CdS domains (total Gibbs free energy,⁴¹ $\Delta G^0 > 1$ eV), matching electron momenta in conduction band edges of both crystal phases, and relatively low mismatch of lattice parameters at the interface (2.7%). The characteristic transition time corresponding to the transfer of more than half of electron population that initially resides in the ZnSe domain into CdS NRs was calculated according to the following equation,

$$\frac{\Delta A_{\text{donor}}(t=0) \times \Delta A_{\text{acceptor}}(t)}{\Delta A_{\text{acceptor}}(t=0) \times \Delta A_{\text{donor}}(t)} = 2 \quad (1a)$$

where $\Delta A_{\text{acceptor}}$ is the combined state-filling bleach of all acceptor excitons ($1P_{CdS} + 1S_{CdS}$), ΔA_{donor} is an integrated bleach signal of donor excitons ($1S_{ZnSe}$), and $t = 0$ is the earliest time, for which measurements of the bleach can be considered reliable (here, $t = 200$ fs). Using eq 1, we estimate the characteristic electron transfer time to be less than 350 fs.

Selective excitation of carriers into the CdS domain of ZnSe/CdS barbells was performed using 420-nm pump pulses, for which photon energies fall below the band gap of ZnSe tips. According to the energy diagram in Figure 4b, these photons can only be absorbed through the excitation of $1S$ and $1P$ excitonic transitions in CdS NRs, while excited states of the ZnSe component remain essentially unoccupied. Experimental evidence of the selective carrier injection into CdS portion of barbells is seen in the TA spectra, where the early time bleach occurs primarily in the spectral range of the lower-energy $1S_{CdS}$ transition. In addition to strong bleach in CdS, a weak negative signal was also observed in the wavelength range of the $1S_{ZnSe}$ transition, the en-

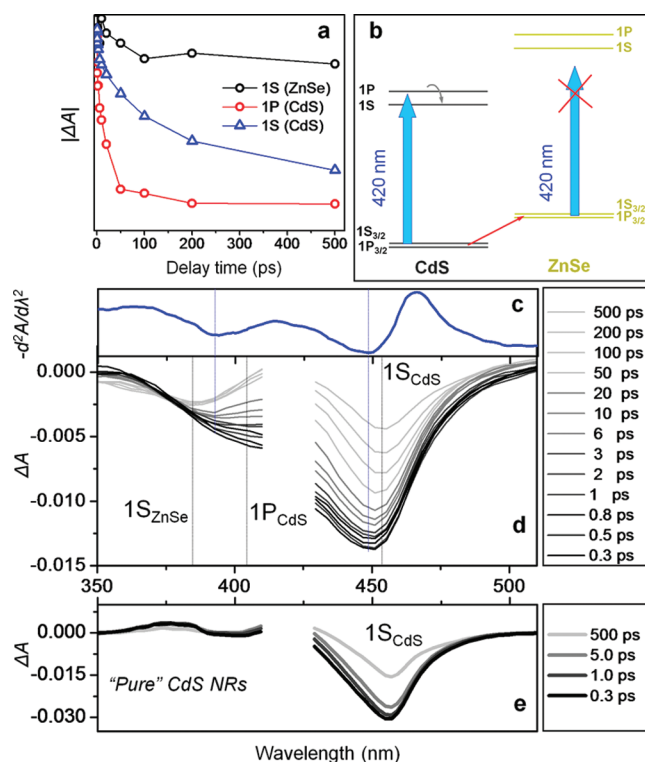


Figure 4. TA measurements of ZnSe/CdS barbells resulting from selective excitation of CdS domains ($\lambda_{\text{pump}} = 420$ nm): (a) temporal dynamics of the TA bleach recovery for $1S(e)–1S_{3/2}(h)$ excitons in ZnSe (black), $1P(e)–1P_{3/2}(h)$ excitons in CdS (red), and $1S(e)–1S_{3/2}(h)$ excitons in CdS (blue); (b) energy diagram of electronic states showing the maximum energy of pump photons (blue arrows) under selective excitation of CdS domains. Note that the average photon energy is not sufficient to induce absorption in ZnSe; (c) second derivative of the absorption profile; (d) TA spectra of ZnSe/CdS barbells resulting from $\lambda_{\text{pump}} = 420$ nm excitation pulses; (e) TA spectra of pure CdS NRs ($\lambda_{\text{pump}} = 420$ nm).

ergy of which lies 0.3 eV above those of excitation photons (Figure 4d). Such above-the-threshold bleach was attributed to the energy-independent effect of local fields (Stark effect) and not the state filling, as can be inferred by nearly identical behavior of the early time TA curve and the second derivative of the absorption profile (Figure 4c). For instance, the effect of local fields on $1S_{\text{ZnSe}}$ and $1S_{\text{CdS}}$ bleaching signals can be easily identified in early time traces ($\Delta t < 1$ ps) as spectral shifts of both peaks by several nanometers from their longer-delay position ($\Delta t > 100$ ps), as indicated by the offsets of blue and gray lines in Figure 4d. A sizable contribution of Stark effect into TA is also manifested by a remarkable similarity between ΔA ($\Delta t < 1$ ps) and $d^2A/d\lambda^2$ slopes throughout the most of the spectral range.

The contribution of the Stark effect into band edge signals decreases with the time, Δt , such that bleach signals corresponding to delays longer than several picoseconds are primarily due to state filling. A compelling evidence of the diminishing role of the Stark effect is provided by the changing slope of bleach recovery traces over the $\Delta t = 2–10$ ps time window and the gradual shift of the $1S_{\text{CdS}}$ and $1S_{\text{ZnSe}}$ spectral positions toward the steady-state values. Interestingly, the subse-

quent decay of $1S_{\text{CdS}}$ excitons is accompanied by further red-shifting of ΔA minimum that persist for another 200 ps. At this delay, the contribution of the Stark effect into the bleach is insignificant, which suggests that a different mechanism is responsible for the observed red-shift. One possible explanation of this phenomenon was presented in our earlier work on dot-in-a-rod heterostructures²⁸ showing that such slow recovery of the spectral minimum can be explained in terms of Coulomb energy of the charge-separated state, $1S_{\text{h}}(\text{ZnSe})–1S_{\text{e}}(\text{CdS})$. Due to quantum confinement effects, the energy of e–h interaction in nanocrystals is inversely proportional to the square of the confinement length, a , such that $\Delta E = -(h^2/8m_e a^2)$. Since the delocalization of the hole wave function into ZnSe material is rather slow, the confinement length increases gradually, causing a lingering red-shift in the position of $1S_{\text{CdS}}$ bleach (since m_{h} is greater than m_{e} , the Coulomb interaction-induced shift of the hole level in ZnSe is less pronounced).

The early time recovery of the $1S$ bleach in the ZnSe material is accompanied both by the changing slope of recovery traces and by the gradual shift of ΔA minimum toward the steady-state value of 384 nm, which is expected due to the diminishing contribution of the Stark effect. The subsequent decay of this transition, however, occurs at a surprisingly slow rate (see Figure 4a), which cannot be attributed to carrier relaxation alone. Indeed, the initial bleach of $1S_{\text{ZnSe}}$ occurs primarily due to the Stark effect and not state filling since the energy of pump photons is not sufficient to reach across the band gap of ZnSe. Nevertheless, the state filling component is clearly present in the longer-delay spectra. Moreover, the intensity of this band remains nearly constant in the 100–500 ps time interval, which strongly suggests repopulation of $1S$ states even after all the above lying levels in ZnSe are clearly depleted.

According to the energy diagram in Figure 4, the only excited state that has the sufficient energy to in-

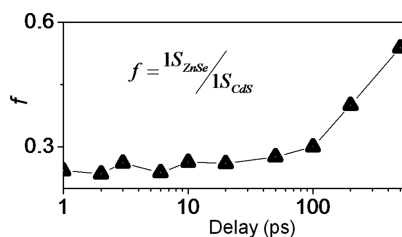


Figure 5. The ratio of $1S_{\text{ZnSe}}$ to $1S_{\text{CdS}}$ excitons as a function of pump–probe delay. The increase of f supports the assumption that the delayed bleaching of $1S_{\text{ZnSe}}$ transitions occurs due to hole transfer from the band edge of CdS into that of ZnSe.

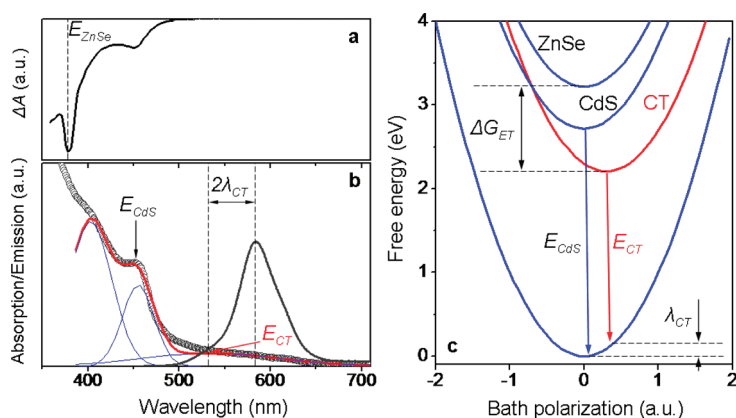


Figure 6. Modeling free energy curves associated with the charge transfer in ZnSe/CdS barbells: (a) fragment of the TA spectrum showing the energy of the ZnSe band edge transition (b) analysis of the emission and absorption transitions in ZnSe/CdS barbells; (c) free energy curves for the ZnSe, CdS, and charge transfer (CT) bands versus bath polarization obtained from the analysis of barbell spectra.

ject carriers into $1S_{\text{ZnSe}}$ and remains populated at times longer than 100 ps is a valence band edge in the CdS portion of a barbell. The transition of holes from $1S_{\text{h}}(\text{CdS})$ to $1S_{\text{h}}(\text{ZnSe})$ levels is exothermic and is expected to produce a delayed repopulation of ZnSe, manifested by the $1S_{\text{ZnSe}}$ bleach. Such hole-transfer scenario is also consistent with the increasing ratio of $1S_{\text{ZnSe}}$ to $1S_{\text{CdS}}$ signals with the pump–probe delay (Figure 5), which corroborates a correlation between the onset of excited state bleach in the ZnSe domain and a decrease of carrier population in CdS NRs. We note that a contribution of holes into ΔA is less than that of electrons, as expected due to high hole-to-electron effective mass ratios, but it is not zero. For instance, hole-induced bleaching of the above-the-pump-energy transition has been observed previously in a CdSe/CdS heterostructured system.²⁷ Considering the fact that $1S_{\text{ZnSe}}$ states are initially not occupied and the delayed bleaching of these transitions correlates well with the recovery of the CdS bleach, we conclude that resonant pumping of the CdS NRs results in the transfer of photoinduced holes into the ZnSe domain. This conclusion is strongly supported by the fact that “pure” CdS NRs do not show any bleach in the vicinity of $\lambda = 384$ nm. Using eq 1, we estimate the characteristic time for the observed hole transfer to be 95 ps, which is much slower than transfer of electrons from ZnSe into CdS observed under resonant pumping of the $1S_{\text{ZnSe}}$ transitions.

To better understand the mechanism of charge transfer in ZnSe/CdS barbells we evaluate the basic thermodynamic parameters for this system within the framework of Marcus theory.⁴¹ This approach can provide an intuitive picture of photoinduced electron transfer (ET) through interplay of the free energy difference between the reactants and products, ΔG^0 , and the extent of reorganization that the environment must undergo to accommodate the change in charge distri-

bution, λ (reorganization energy). Depending on these parameters, Marcus theory identifies three distinct regimes of ET that include normal ($-\Delta G^0 < \lambda$), for which the ET rate increases with increasing driving free energy for the reaction, barrierless ($-\Delta G^0 = \lambda$), for which a maximum rate is observed, and inverted ($-\Delta G^0 > \lambda$), for which the ET rate decreases despite increasing exothermicity driving the reaction.

The main idea of our analysis is to identify a specific regime of ET occurring in fabricated barbells by constructing free energy curves that represent different states of the system as quadratic functions of bath polarization.⁴² As was recently demonstrated by Scholes *et al.*,⁴³ such qualitative description of electronic processes in heterostructured NCs can be derived from steady-state emission and absorption spectra provided that the signature of the charge transfer bands can be identified in optical measurements. Within this approach, the reorganization energy associated with an interfacial electron transfer is given approximately as half the Stokes shift between spatially indirect absorption and emission energies, which, in this study, correspond to spectral values of 535 and 583 nm, respectively (Figure 6b). Using this information, we can plot the free energy curves (Figure 6c) for electronic states in ZnSe, CdS, and charge transfer (CT) bands relative to the ground state, calculated as quadratic functions of coordinate x :⁴⁴

$$G_i(x) = \frac{1}{2}(x - \sqrt{2\lambda_i})^2 + \Delta G_i^0 \quad (2)$$

where the harmonic force constant is set to unity, and ΔG_i^0 is the free energy difference between ground state and excited state i , given by the energy of the absorption peak E_i minus the reorganization energy λ_i .

To determine the Stokes shifts for all three excitation bands we have assumed that inhomogeneous broadening of absorption and emission lines corresponds to a Gaussian shape, which represents the case of weakly correlated transitions.⁴⁵ By fitting the absorption and emission CT bands in Figure 6b, we found that the reorganization energy required for the electron transfer from ZnSe to CdS is 94 meV. On the basis of the fact that the free energy difference, ΔG_i^0 , for this band is -1.03 eV, we conclude that the charge transfer reaction occurs in the Marcus inverted region, ($-\Delta G^0 > \lambda$). Similar results were also found for the case of CdSe/CdTe nanobarbells, where the inverted regime of ET was attributed to the weak exciton–phonon coupling in semiconductor NCs.⁴³

In conclusion, we have used transient absorption spectroscopy to study the dynamics of photoinduced charge transfer in type II heterostructured nanocrystals comprising a barbell-like arrangement of ZnSe and CdS semiconductors. Experimental data provides strong evidence for photoinduced charge transfer between the two nanocrystalline domains, which can be controlla-

bly performed in either direction by modulating the excitation wavelength, such that the resonant excitation of carriers in the ZnSe material leads to 350 fs injection of electrons into CdS, and the excitation of carriers in the CdS portion of barbells results in a slower transfer

of holes into ZnSe. A qualitative thermodynamic description of observed electron processes within the classical limit of Marcus theory was subsequently used to show that the charge transfer reaction between ZnSe into CdS domains occurs in the Marcus inverted region.

EXPERIMENTAL SECTION

Chemicals. Sulfur (99.999%, Acros), 1-octadecene (ODE, tech., 90%, Aldrich), cadmium oxide (99.99%, Aldrich), oleic acid (OA, tech., 90%, Aldrich), tri-*n*-octylphosphine (TOP, 97%, Aldrich), tri-*n*-octylphosphine oxide (TOPO, 99%, Aldrich), *n*-octadecylphosphonic acid (ODPA, PCI Synthesis), *n*-hexylphosphonic acid (HPA, PCI Synthesis), octadecylamine (ODA, 90%, tech., Acros), zinc oxide (99+%, Aldrich), selenium (99.5+%, Acros), hexane (anhydrous, 95%, Aldrich), methanol (99.8+%, EMD), toluene (anhydrous, 99.8%, Aldrich), chloroform (anhydrous, 99+%, Aldrich). All chemicals were used as received without any further purification.

Synthesis of ZnSe/CdS barbells. ZnSe/CdS barbells were fabricated by growing ZnSe tips onto previously prepared CdS nanorods (NRs). To achieve a moderate dispersion of NR widths, CdS NRs were synthesized using a seeded-type approach by introducing small-diameter CdS NCs into the reaction mixture for nucleating the growth of linear CdS extensions, according to the procedure adapted from ref 15. Original CdS seeds were not distinguishable in fabricated CdS NRs.

The amount of CdS seeds for the synthesis of CdS NRs, fabricated according to ref 46 was calculated using an empirical approach, whereby the product of the particle absorption at 400 nm (excitonic feature) and the volume of the colloidal suspension (in mL) was set to be in the range of 5–15. In a typical synthesis of CdS NRs, CdS seed powder was dispersed in 1.8 mL of TOP and subsequently introduced (at 60 °C) into the sulfur injection solution, previously prepared by dissolving sulfur (0.120 g) in TOP (1.81 mL) at 200 °C. Separately, the mixture of cadmium oxide (0.060 g), TOPO (3.0 g), ODPA (0.290), and HPA (0.080 g) in a 50 mL 3-neck flask was exposed to vacuum at 150 °C for ca. 30 min. Subsequently, the system was switched to Ar flow and heated to above 350 °C until the solution turned optically clear and colorless. At this point, TOP (1.81 mL) was added to the flask as the Cd precursor coordinating solvent. The nanorod growth was initiated by a quick injection of the seed/sulfur solution at 380 °C. After the temperature recovered to 350 °C the nanorods were allowed to grow for an additional 7–9 min. Purification of CdS NRs was similar to those of CdS seeds.

In a typical synthesis of ZnSe/CdS barbells, 0.5 mL of hexane-suspended CdS NRs (60 times diluted injection solution showed the excitonic absorption peak of 0.75, which corresponds to approximately 12 mg of dry nanorods) were injected into a degassed mixture of ODE (6.0 mL) and ODA (1.5 g) at 80 °C and pumped for about 20 min to remove hexane and any residual air from the system. At this step, the system was switched to Ar flow and heated to 250 °C before injecting the precursors. Zinc injection solution was prepared by heating zinc oxide (0.0350 g), OA (1.2 mL), and TOP (1.5 mL) to above 250 °C until the solution was clear. Subsequently, it was allowed to cool to about 60 °C and mixed with the Se:TOP precursor (0.0340 g of selenium and 0.7 mL of TOP). During the nanobarbell growth the precursor solution was added *via* syringe to the reaction flask kept at 245 °C in 0.1 mL amounts every 2 min. After 10–20 min, the reaction was stopped by cooling the flask to ca. 50 °C and adding excess toluene. Subsequent cleaning was done using hexane/methanol extraction.

Characterization. UV–vis absorption and photoluminescence spectra were recorded using CARY 50 scan spectrophotometer and Jobin Yvon Fluorolog FL3-11 fluorescence spectrophotometer. High resolution transmission electron microscopy measurements were carried out using JEOL 3011UHR operated at 300 kV.

Transient Absorption Spectroscopy. The experimental setup was based on the Ti:sapphire amplified laser system operating at a repetition rate of 1 kHz, the output of which was split into

two components: one was directed to the TOPAS optical parametric amplifier to produce excitation pulses, and the second one was focused onto a CaF₂ plate to generate a white-light-continuum for broad-band probe pulses (see the Supporting Information). All transient absorption data were corrected for the group velocity dispersion of the white-light continuum by using the nonresonant signals of pure solvents. The incident excitation beam was attenuated before the sample (0.2 mm flow cell) to ensure a linear pump power dependence of the CdS bleach signal at early probe times ($t \approx 1$ ps) (see Figure SF1 in the Supporting Information section). A typical excitation pulse power was 1.5 μ J per pulse at the sample position with an average beam diameter of 300 μ m. We estimate that the average number of excitations per nanocrystal is near unity, $\langle N \rangle = j\sigma \approx 1$, where j is the pump fluence and σ is the absorption cross section at the pump wavelength, estimated using known extinction coefficients for CdS colloids⁴⁷ (e.g., for $\lambda_{\text{exc}} = 420$ nm, $\sigma = 2 \times 10^{-15}$ cm²). The pump–probe cross correlation width was 200 fs fwhm.

Acknowledgment. We gratefully acknowledge Bowling Green State University for financial support (Grants SF07, RIC2009, RCE2008).

Supporting Information Available: Experimental details. This material is available free of charge *via* the Internet at <http://pubs.acs.org>.

REFERENCES AND NOTES

- Rajeshwar, K.; Tacconi, N. R. D.; Chenthamarakshan, C. R. Semiconductor-Based Composite Materials: Preparation, Properties, and Performance. *Chem. Mater.* **2001**, *13*, 2765–2782.
- Cozzoli, P. D.; Pellegrino, T.; Manna, L. Synthesis, Properties and Perspectives of Hybrid Nanocrystal Structures. *Chem. Soc. Rev.* **2006**, *35*, 1195–1208.
- Kumar, S.; Jones, M.; Lo, S. S.; Scholes, G. D. Nanorod Heterostructures Showing Photoinduced Charge Separation. *Small* **2007**, *3*, 1633–1639.
- Kim, S.; Fisher, B.; Eisler, H. J.; Bawendi, M. Type-II Quantum Dots: CdTe/CdSe (Core/Shell) and CdSe/ZnTe (Core/Shell) Heterostructures. *J. Am. Chem. Soc.* **2003**, *125*, 11466–11467.
- Schöps, O.; Thomas, N. L.; Woggon, U.; Artemyev, M. V. Recombination Dynamics of CdTe/CdS Core–Shell Nanocrystals. *J. Phys. Chem. B* **2006**, *110*, 2074–2079.
- Yu, K.; Zaman, B.; Romanova, S.; Wang, D. Ripmeester, Sequential Synthesis of Type II Colloidal CdTe/CdSe Core–Shell Nanocrystals. *Small* **2005**, *1*, 332.
- Xie, R.; Zhong, X.; Basché, T. Synthesis Characterization, and Spectroscopy of Type-II Core/Shell Semiconductor Nanocrystals with ZnTe Cores. *Adv. Mater.* **2005**, *17*, 2741–2745.
- Cheng, C. T.; Chen, C. Y.; Lai, C. W.; Liu, W. H.; Pu, S. C.; Chou, P. T.; Chou, Y. H.; Chiu, H. T. Syntheses and Photophysical Properties of Type-II CdSe/ZnTe/ZnS (Core/Shell/Shell) Quantum Dots. *J. Mater. Chem.* **2005**, *15*, 3409–3414.
- Danek, M.; Jensen, K. F.; Murray, C. B.; Bawendi, M. G. Synthesis of Luminescent Thin-Film CdSe/ZnSe Quantum Dot Composites Using CdSe Quantum Dots Passivated with an Overlayer of ZnSe. *Chem. Mater.* **1996**, *8*, 173–180.

10. Ivanov, S. A.; Nanda, J.; Piryatinski, A.; Achermann, M.; Balet, L. P.; Bezel, I. V.; Anikeeva, P. O.; Tretiak, S.; Klimov, V. I. Light Amplification Using Inverted Core/Shell Nanocrystals: Towards Lasing in The Single-Exciton Regime. *J. Phys. Chem. B* **2004**, *108*, 10625–10630.
11. Ivanov, S. A.; Piryatinski, A.; Nanda, J.; Tretiak, S.; Zavadil, K. R.; Wallace, W. O.; Werder, D.; Klimov, V. I. Type-II Core/Shell CdS/ZnSe Nanocrystals: Synthesis, Electronic Structures, and Spectroscopic Properties. *J. Am. Chem. Soc.* **2007**, *129*, 11708–11719.
12. Nemchinov, A.; Kirsanova, M.; Hewa-Kasakarage, N. N.; Zamkov, M. Synthesis and Characterization of Type II ZnSe/CdS Core/Shell Nanocrystals. *J. Phys. Chem. C* **2008**, *112*, 9301–9307.
13. Reiss, P.; Protiere, M.; Li, L. Core/Shell Semiconductor Nanocrystals. *Small* **2009**, *5*, 154–168.
14. Pandey, A.; Guyot-Sionnest, P. Intraband Spectroscopy and Band Offsets of Colloidal II–VI Core/Shell Structures. *J. Chem. Phys.* **2007**, *127*, 104710.
15. Carbone, L.; Nobile, C.; De Giorgi, M.; Sala, F. D.; Morello, G.; Pompa, P.; Hytch, M.; Snoeck, E.; Fiore, A.; Franchini, I. R.; et al. Synthesis and Micrometer-Scale Assembly of Colloidal CdSe/CdS Nanorods Prepared by a Seeded Growth Approach. *Nano Lett.* **2007**, *7*, 2942–2950.
16. Dorfs, D.; Salant, A.; Popov, I.; Banin, U. ZnSe Quantum Dots Within CdS Nanorods: A Seeded-Growth Type-II System. *Small* **2008**, *4*, 1319–1323.
17. Hewa-Kasakarage, N. N.; Kirsanova, M.; Nemchinov, A.; Schmall, N.; El-Khoury, P. Z.; Tarnovsky, A. N.; Zamkov, M. Radiative Recombination of Spatially Extended Excitons in (ZnSe/CdS)/CdS Heterostructured Nanorods. *J. Am. Chem. Soc.* **2009**, *131*, 1328–1334.
18. Shieh, F.; Saunders, A. E.; Korgel, B. A. General Shape Control of Colloidal CdS, CdSe, CdTe Quantum Rods and Quantum Rod Heterostructures. *J. Phys. Chem. B* **2005**, *119*, 8539–8542.
19. Halpert, J. E.; Porter, V. J.; Zimmer, J. P.; Bawendi, M. G. Synthesis of CdSe/CdTe Nanobarbells. *J. Am. Chem. Soc.* **2006**, *128*, 12590–12591.
20. Kirsanova, M.; Nemchinov, A.; Hewa-Kasakarage, N. N.; Schmall, N.; Zamkov, M. Synthesis of ZnSe/CdS/ZnSe Nano-Barbells Showing Photoinduced Charge Separation. *Chem. Mater.* **2009**, *21*, 4305–4309.
21. Shi, W.; Zeng, H.; Sahoo, Y.; Ohulchanskyy, T. Y.; Ding, Y.; Wang, Z. L.; Prasad, P. N. A General Approach to Binary and Ternary Hybrid Nanocrystals. *Nano Lett.* **2006**, *6*, 875–881.
22. Yu, H.; Chen, M.; Rice, P. M.; Wang, S. X.; White, R. L.; Sun, S. Dumbbell-like Bifunctional Au-Fe₃O₄ Nanoparticles. *Nano Lett.* **2005**, *5*, 379–382.
23. Carbone, L.; Kudera, S.; Carlino, E.; Parak, W. J.; Giannini, C.; Cingolani, R.; Manna, L. Multiple Wurtzite Twinning in CdTe Nanocrystals Induced by Methylphosphonic Acid. *J. Am. Chem. Soc.* **2006**, *128*, 748–755.
24. Milliron, D. J.; Hughes, S. M.; Cui, Y.; Manna, L.; Li, J.; Wang, L.; Alivisatos, A. P. Colloidal Nanocrystal Heterostructures with Linear and Branched Topology. *Nature* **2004**, *430*, 190–195.
25. Peng, P.; Milliron, D. J.; Hughes, S. M.; Johnson, J. C.; Alivisatos, A. P.; Saykally, R. J. Femtosecond Spectroscopy of Carrier Relaxation Dynamics in Type II CdSe/CdTe Tetrapod Heteronanostructures. *Nano Lett.* **2005**, *5*, 1809–1813.
26. Dooley, C. J.; Dimitrov, S. D.; Fiebig, T. Ultrafast Electron Transfer Dynamics in CdSe/CdTe Donor–Acceptor Nanorods. *J. Phys. Chem. C* **2008**, *112*, 12074–12076.
27. Lupo, M. G.; Sala, F. D.; Carbone, L.; Zavelani-Rossi, M.; Fiore, A.; Luthser, L.; Polli, D.; Cingolani, R.; Manna, L.; Lanzani, G. Ultrafast Electron-Hole Dynamics in Core/Shell CdSe/CdS Dot/Rod Nanocrystals. *Nano Lett.* **2008**, *8*, 4582–4587.
28. Hewa-Kasakarage, N. N.; El-Khoury, P. Z.; Schmall, N.; Kirsanova, M.; Nemchinov, A.; Tarnovsky, A. N.; Bezryadin, A.; Zamkov, M. The Effect of Dielectric Friction on The Rate of Charge Separation in Type II ZnSe/CdS Semiconductor Nanorods. *App. Phys. Lett.* **2009**, *94*, 133113–133115.
29. Grätzel, M. Photoelectrochemical Cells. *Nature* **2001**, *414*, 338–344.
30. Miller, D. A. B.; Chemla, D. S.; Damen, T. C.; Gossard, A. C.; Wiegmann, W.; Wood, T. H.; Burrus, C. A. Band-Edge Electroabsorption in Quantum Well Structures—The Quantum-Confined Stark Effect. *Phys. Rev. Lett.* **1984**, *53*, 2173–2176.
31. Kuo, Y.; Lee, Y. K.; Ge, Y.; Ren, S.; Roth, J. E.; Kamins, T. I.; Miller, D. A.; Harris, J. S. Strong Quantum-Confined Stark Effect in Germanium Quantum-Well Structures on Silicon. *Nature* **2005**, *437*, 1334.
32. Reiss, P. ZnSe Based Colloidal Nanocrystals: Synthesis, Shape Control, Core/Shell, Alloy and Doped Systems. *New J. Chem.* **2007**, *31*, 1843–1852.
33. Dinger, A.; Petillon, S.; Grun, M.; Hetterich, M.; Klingshirm, C. Conduction Band Offset of The CdS ZnSe Heterostructure. *Semicond. Sci. Technol.* **1999**, *14*, 595–598.
34. Hunsche, S.; Dekorsy, T.; Klimov, V.; Kurz, H. Ed.-in-Chief; Landolt-Boernstein: Numerical Data and Functional Relationships in Science and Technology. Group III; Springer Verlag: Berlin, 1998.
35. Hunsche, S.; Dekorsy, T.; Klimov, V.; Kurz, H. Ultrafast Dynamics of Carrier-Induced Absorption Changes in Highly-Excited CdSe Nanocrystals. *Appl. Phys. B: Laser Opt.* **1996**, *62*, 3–10.
36. Ekimov, A. I.; Hache, F.; Schanne-Klein, M. C.; Ricard, D.; Flytzanis, C.; Kudryavtsev, I. A.; Yaveza, T. V.; Rodina, A. V.; Efros, A. L. Absorption and Intensity-Dependent Photoluminescence Measurements On CdSe Quantum Dots: Assignment of The First Electronic Transitions. *J. Opt. Soc. Am. B* **1993**, *10*, 100–106.
37. Nirmal, M.; Norris, D. J.; Kuno, M.; Bawendi, M. G.; Efros, A. L.; Rosen, M. Observation of The Dark Excitons in CdSe Quantum Dots. *Phys. Rev. Lett.* **1995**, *75*, 3728–3731.
38. Klimov, V.; Hunsche, S.; Kurz, H. Biexciton Effects in Femtosecond Nonlinear Transmission of Semiconductor Quantum Dots. *Phys. Rev. B* **1994**, *50*, 8110–8113.
39. Klimov, V. I. Optical Nonlinearities and Ultrafast Carrier Dynamics in Semiconductor Nanocrystals. *J. Phys. Chem. B* **2000**, *104*, 6112–6123.
40. Norris, D.; Sacra, A.; Murray, C.; Bawendi, M. Measurement of the Size Dependent Hole Spectrum in CdSe Quantum Dots. *Phys. Rev. Lett.* **1994**, *72*, 2612–2615.
41. Marcus, R. A.; Sutin, N. Electron Transfers in Chemistry and Biology. *Biochim. Biophys. Acta* **1985**, *811*, 265–322.
42. Stratt, R. M.; Maroncelli, M. Nonreactive Dynamics in Solution: The Emerging Molecular View of Solvation Dynamics and Vibrational Relaxation. *J. Phys. Chem.* **1996**, *100*, 12981–12996.
43. Scholes, G. D.; Jones, M.; Kumar, S. Energetics of Photoinduced Electron-Transfer Reactions Decided by Quantum Confinement. *J. Phys. Chem. C* **2007**, *111*, 13777–13785.
44. Marcus, R. A. Relation Between Charge-Transfer Absorption and Fluorescence-Spectra and The Inverted Region. *J. Phys. Chem.* **1989**, *93*, 3078–3086.
45. Fleming, G. R.; Cho, M. Chromophore-Solvent Dynamics. *Annu. Rev. Phys. Chem.* **1996**, *47*, 109–134.
46. Yu, W. W.; Peng, X. Formation of High-Quality CdS and Other II–VI Semiconductor Nanocrystals in Noncoordinating Solvents: Tunable Reactivity of Monomers. *Angew. Chem.* **2002**, *41*, 2368–2371.
47. Yu, W. W.; Qu, L.; Guo, W.; Peng, X. Experimental Determination of the Extinction Coefficient of CdTe, CdSe, and CdS Nanocrystals. *Chem. Mater.* **2003**, *15*, 2854–2860.